Derivative Target Line (DTL) for Continuous Human Activity Detection and Recognition

Guendel, Ronny G.; Fioranelli, Francesco; Yarovoy, Alexander

DOI
10.1109/RadarConf2043947.2020.9266383

Publication date
2020

Document Version
Final published version

Published in
2020 IEEE Radar Conference, RadarConf 2020

Derivative Target Line (DTL) for Continuous Human Activity Detection and Recognition

Ronny G. Guendel, Francesco Fioranelli, Alexander Yarovoy
Microwave Sensing, Signals and Systems (MS3), Delft University of Technology, Delft, Nederland
r.guendel, f.fioranelli, a.yarovoy@tudelft.nl

***Abstract*—In this paper, we investigate the classification of Activities of Daily Living (ADL) by using a pulsed ultra-wideband radar. Specifically, we focus on contiguous activities that can be inseparable in time and share a common transition, such as walking and falling. The range-time data domain is deliberately exploited to determine transitions from translation activities to in-place activities and vice versa, using a simple, yet effective approach based on the proposed Derivative Target Line (DTL). The separation of different in-place activities is then addressed using an energy detector finding the onset and offset times. Furthermore, the possible ADL for classification are limited at any decision stage based on kinematic constraints of human movements. We show that such limitation of classes at any given time leads to a classification improvement over a classifier containing always all ADL classes.**

***Index Terms*—micro-Doppler, assisted living, feature fusion, machine learning, classification, range-map, activities of daily living.**

I. Introduction

Nowadays, aging of the population with an increasing number of elderly people becomes one of the top societal challenges since the elderly live longer at home with chiefly limited external support. Remotely monitoring systems using Radio Frequency (RF) technologies are powerful non-obtrusive tools for Activities of Daily Living (ADL) [1]. Different approaches with different radars have shown promising results, e.g. Continuous Waveform (CW) or Frequency Modulated Continuous Waveform (FMCW) and pulsed ultra-wideband (UWB) radars, where the former provides a micro-Doppler (μD) spectrogram only, whereas the latter two support diverse data representations such as the range-time, range-Doppler, or radar data cube processing [2]–[4]. Radar capability improvements in terms of operational bandwidth allow for monitoring of vital signs (heart rate or respiration rate) thanks to the finer radar resolution, both in the range and frequency domain [5]. Approaches with sensor fusion, e.g. wearable devices or recognition with multiple cooperative radars, can be used to increase the monitoring accuracy and generally improves the overall performance by exploiting advantages of diverse sensors [6]–[9].

This paper investigates the classification of sequences for ADL using the range and Doppler information provided by a pulsed UWB radar, and specifically where the transition between translational movement (e.g. walking) and in-place movements (e.g. bending or sitting) can be separated. We propose an algorithm monitoring the person in an indoor environment, where we deliberately exploit the range-time profile for the discrimination of translating vs in-place behaviors. The algorithm reduces the noise outside the true Target Line (TL) and monitors the position of the subject over time. This method can be used for data sequences of any length and does not require a time limitation as in [10]. The proposed Derivative Target Line (DTL) is then used and combined with the limitation of the possible classes for classification. This, with different classifiers and optimization of their parameters, is shown to significantly improve the classification rate compared to using all classes at any given time. We adopt Two Dimensional (2D) Principal Component Analysis (PCA) as a feature extractor, and the decision tree classifier for both, the micro-Doppler (μD), the range-map (RM), and their fusion.

The rest of the paper is organized as follows. Section II introduces the radar setup, data analysis, and the proposed algorithm. Section III describes the data acquisition procedure and the classification performance achieved with our experimental data. The conclusion and remarks are given in Section IV.

II. Data Analysis

The results presented in this paper use a P410 Humatics radar (former Time Domain™). The pulsed radar has a bandwidth of 2 GHz and a center frequency of 4.3 GHz [11], [12]. The coverage area is 4.39 m from 1 m to 5.39 m, as shown in the RM in Fig. 1a. The radar was used with a pulse repetition interval of 8.2 ms, with an unambiguous Doppler frequency of ± 61 Hz. The Short-time Fourier transform (STFT) is used [13], [14] with a Hann (Hanning) window of 64 samples and an overlap of 60 samples (94%) to compute the μD spectrogram, as in Fig 4b. The majority of the noise samples from the μD spectrogram and the RM is then eliminated by using the eCLEAN algorithm [4], [15]. The initial μD spectrogram and RM (Fig. 1a) are resized to 128 sampled for the y-axis and 64 samples for 1 s in slow time, which results to 3840 samples for the 60 s sequence. The finally resulting μD spectrogram and RM are shown in Fig. 4a and 4b.

A. Target Line (TL) Detection

The RM contains essential information on the human movements, such as acceleration in either directions for translating

978-1-7281-8942-0/20$31.00 © 2020 IEEE

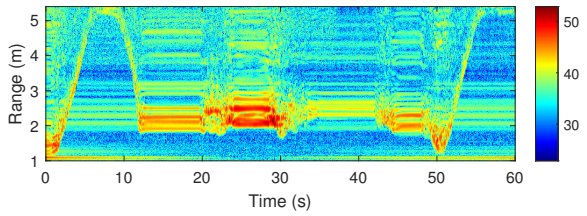

(a) RM before post-processing.

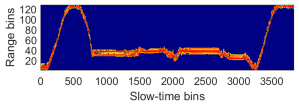

(b) Cleaned RM (RMC).

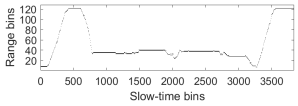

(c) Target Line of the RMC.

Fig. 1: (a) The raw range-map (RM) together with (b) the cleaned RM (RMC) and (c) the Target Line (TL) for the activity sequence of a bi-directional walking merged with falling, followed by standing up from a fall, sitting down, standing up, and finally a bi-directional walking again.

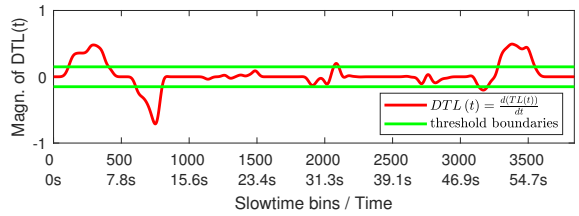

(a) DTL with thresholds.

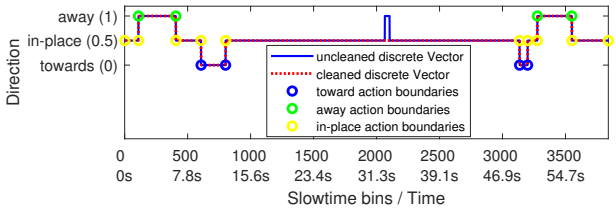

(b) DV of the DTL with the boundary points.

Fig. 2: The Derivative Taget Line (DTL) and the Decision Vector (DV) for translating in either direction and the in-place activity segments.

activities, towards or away from the radar, or for the non-translating activities. This allows to find the onset and offset of each inter class activities, e.g. walking-falling merged [10]. We introduce the Target Line (TL) detection process for finding the position of the target (human being). As a simple cleaning algorithm, a method similar to the TL detection was introduced in the prior work [16]. Our extended method in this paper additionally monitors the position of the target at any given slow-time sample. The cleaned range-map (RMC) is shown in Fig. 1b and the TL plot can be seen in Fig. 1c.

B. Derivative Target Line (DTL) processing

The initial Target Line vector, $TL(n)$, enables the discrimination between translation and in-place activities since the relative distance to the radar is tracked. For that, we assume that the vector $TL(n)$ is represented by a continuous function $TL(t)$, where t represents the continuous time. Here, the first derivative of $TL(t)$ can be expressed as,

$$DTL\,(t) = \frac{d\,(TL\,(t))}{dt}, \qquad t \in \mathbb{R} : [0s, 60s] \tag{1}$$

with $DTL(t)$ as a function of t representing the slope of the $TL(t)$ at any given time. Particularly, the first derivative of the location (TL) represents the target velocity, which is estimated more precisely without using the μD spectrogram.

As the vector $TL(n)$ is a discretely sampled function, the discrete Derivative Target Line (DTL) can be computed as,

$$DTL\,(n) = TL\,(n+1) - TL\,(n)\,, \qquad n = 0, ..., N-1 \tag{2}$$

The vector $DTL\,(n)$ indicates the person's in-place and translation activities, and is shown in Fig. 2a, as the red curve. The curve refers to the down-sampled RM of 128×3840 samples with a range coverage area between 1 m and 5.39 m for 60 s. The empirically found threshold values of $th = [+0.15, -0.15]$ (green horizontal lines) are used to discriminate between the person's in-place action and the persons translation action in either direction – towards and away from the radar. This is a stand alone experimental result: in the majority of cases, the human velocity in range by the person's in-place action is less than threshold of ± 0.15. The threshold can be decreased to become more sensitive to $th = [+0.10, -0.10]$, for which the false alarm rate of the translation activities increases. On the other hand, a larger threshold ($th = [+0.20, -0.20]$) leads to a more robust system for in-place activities, but with the risk of little swaths in range for translation activities to be easily overlooked. With the DTL and the th, the Decision Vector (DV) is then computed as,

$$DV(n) = \begin{cases} 1, & \text{if } DTL(n) > th(1) = +0.15 \\ 0, & \text{if } DTL(n) < th(2) = -0.15 \\ 0.5, & \text{otherwise} \end{cases} \tag{3}$$

for $n = 1, ..., N-1$ and is shown in Fig. 2b as the blue curve. Specifically, a value of 1 for the DV indicates a translation activity away from the radar, whereas a DV value of 0 shows a translation activity towards the radar. In-place time periods are indicated by 0.5, as shown in Eq. 3. It can be seen that few outliers around the sample 2050 indicate a movement away from the radar, which refers to the backward movement from a standing up after falling. Therefore, small peaks of less than 32 samples (0.5 s) are set to be in-place activities as shown in the Fig. 2b by the red curve. The equivalent values of $DV \in [1, 0, 0.5]$ are shown in the RM and μD spectrogram by the white, gray, and black bars in the Fig. 4a and 4b.

Regarding Fig. 2b, the beginning and ending samples of each sub-sequence – a translation in either directions, or an in-place sequence – is marked with the blue, green, and yellow circles and indicate the onset and offset samples times. In Fig. 2b two translating away activities are found with the offset samples of 406 and 3550. Additionally, there are two

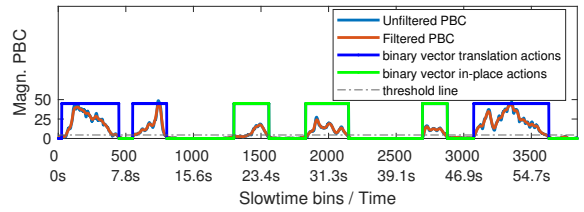

Fig. 3: The Power Burst Curve (PBC) of the sequence where the green and blue lines indicating the onset and offset samples (times) of the in-place and translating activities, respectively.

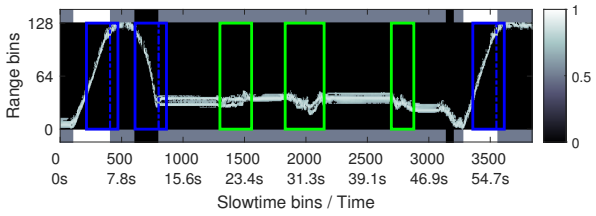

(a) RM with DTL segments.

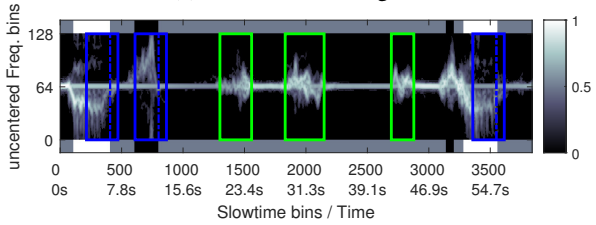

(b) µD with DTL segments.

Fig. 4: The discriminated activities of translating in either direction (blue) and the in-place activities (green) are shown for a multi-motion sequence of 60 s.

translation activities towards the radar denoted by the offset samples of 801 and 3199. The latter does not exceed the time window of 2 s; therefore, the activity is not captured for classification. For the two activities away from the radar and the first activity towards the radar, a window of 4 s (256 samples) is placed, which captures 3 s of the translation activity and 1 s of the in-place activity, as shown by the blue rectangles in Fig. 4a and 4b. The 8-bit gray-scale images of these three specific activities are shown in Fig. 5 with (a), (b), and (f) for the µD and (g), (h), and (l) for the RM.

C. Power Burst Curve (PBC)

The DTL is used to separate translation activities from in-place activities, whereas within in-place activities with almost no range swath the DTL cannot be applied for discriminating between multiple consecutive in-place activities. For separating such in-place activities, we rely on an energy detector, known as the Power Burst Curve (PBC) [13], [17].

Onset and offset times provided by the DTL are used to define the in-place segments. An in-place segment with multiple motions is shown in Fig. 4a and 4b between the sample points 802 and 3135 (12.53 s and 48.98 s). The PBC as in Eq. (8) [18] is applied on the positive frequency bands between 4 Hz and 61 Hz and the negative frequency bands between -4 Hz and -61 Hz. The resulting PBC is shown in Fig. 3 as the blue curve. We apply a moving average window of 20 samples for smoothing the signal, shown as the brown curve (filtered PBC). An empirically found threshold of 5% over the minima has been applied and is computed as, $PBC_{\text{min}} + 0.05 \cdot (PBC_{\text{max}} - PBC_{\text{min}})$. For in-place separation, we only rely on the in-place segment, which means the PBC is not used on any segment which is indicated as a translation activity by the DTL, as discussed before. The discriminated activities are illustrated by the green binary signal vector (binary vector in-place actions). The found onset and offset times are used for cropping the individual spectrogram and RM, as shown in Fig. 4a and 4b indicated with the green rectangles. The saved images for these specific activities are enlarged and shown in Fig. 5 in (c), (d), and (e) for the µD and (i), (j), and (k) for the RM.

III. Experimental Results

The data were collected with six monostatic radars in a linear baseline with 0.5 m separation. The facing angle for the data collection to the radar was within $\pm 51.3°$. In this paper, a multi-activity sequence was chosen with a bi-directional walking contiguously merged with falling at the beginning, followed by a sequence of in-place activities, namely, standing up from a fall, sitting down on a chair, and standing up, before another bi-directional walking ends the sequence. In Fig. 7, the test person performs the activities towards the radar. The test candidates age is between 22 and 40 years, with a height between 1.67m and 1.85m, and a weight between 65kg and 89kg.

For this paper, we are using a comprehensive number of 20 ADL classes which can be found in Table V. A data set of 305 samples for each class was collected using the 6 radar sensors simultaneously, while a training:validation ratio of 80:20 was used. We apply 2D-PCA as a feature extraction method followed by a decision tree classifier [19], [20]. For the 2D-PCA, the covariance matrix H is computed as,

$$H = \frac{1}{I} \sum_{i=1}^{I} (X^{(i)} - \bar{X})^T \cdot (X^{(i)} - \bar{X}) \tag{4}$$

where $\bar{X} \in \mathbb{R}^{\eta \times \eta}$ is the mean image, as $\bar{X} = \frac{1}{I} \sum_{i=1}^{I} X^{(i)}$, with $\eta = 128$ the downsampled image size. I is the total number of images in the training data, and $X^{(i)} \in \mathbb{R}^{\eta \times \eta}$ is the i-th µD or RM image, as shown in Fig. 5, respectively. From the eigendecomposition of H, the eigenvalues and eigenvectors (ν_i) are extracted. The eigenvectors correspond to the d largest eigenvalues form the matrix $\Phi = [\nu_1, \nu_2, ..., \nu_d]$. The default values for d are $d_{\mu\text{D}} = 3$ and $d_{\text{RM}} = 3$ for the µD and the RM classification, respectively.

The training and test images X are projected on the $\eta \times d$-dimensional subspace matrix Φ to compute the principal component matrix, $Y = X\Phi$, for the µD, $Y_{\mu\text{D}}$, with the dimension $\mathbb{R}^{\eta \times d_{\mu\text{D}}}$, and the RM, Y_{RM}, with the dimension dimension $\mathbb{R}^{\eta \times d_{\text{RM}}}$.

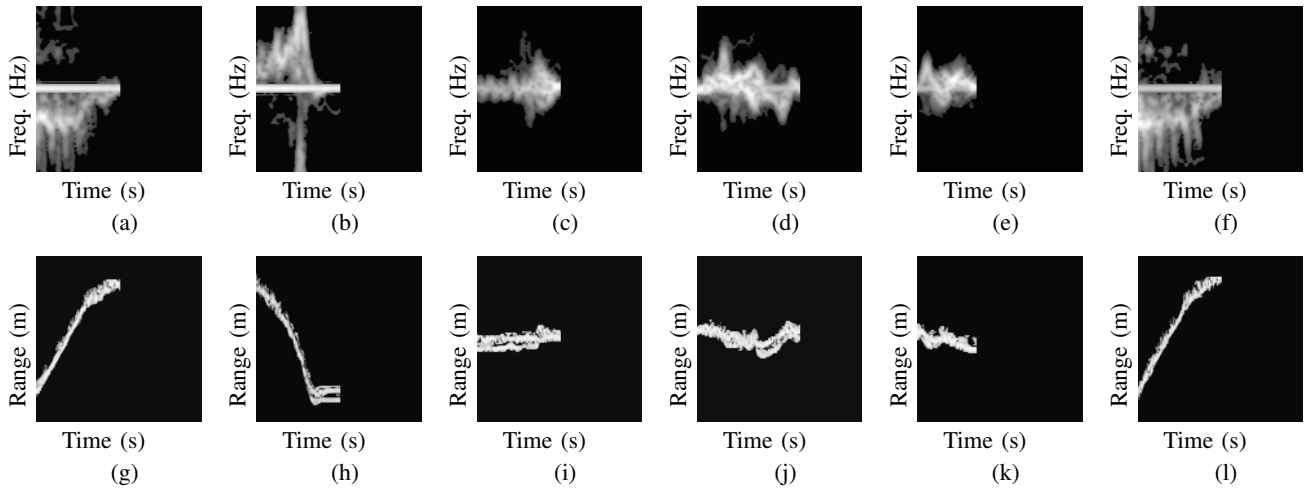

Fig. 5: Captured translation and in-place actions. The subfig. a.-f. show the μD; the subfig. g.-l. the RM, with the activities, namely (a+g) walking away, (b+h) walking-falling towards, (c+i) standing up from falling, (d+j) sitting down, (e+k) standing up from sitting, and (f+l) walking away.

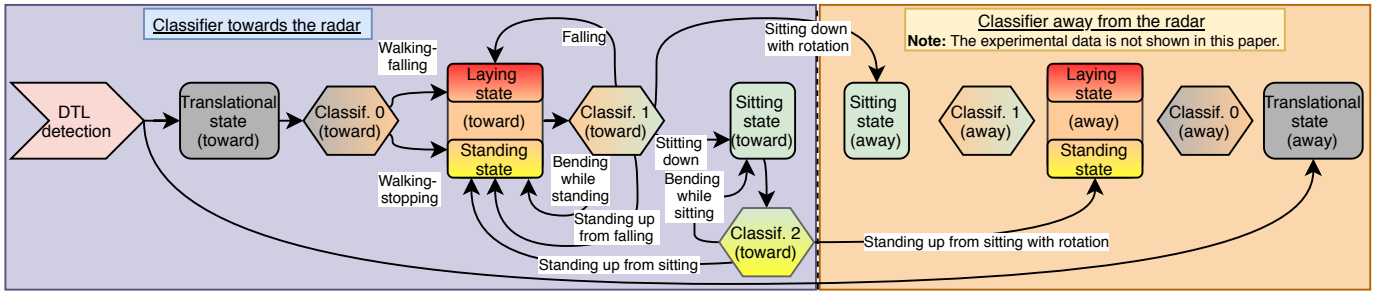

Fig. 6: The classification flow-graph originating from the DTL. The *states* are shown by the square blocks, namely translation, laying, standing, and sitting. The hexagons denote the *classifiers* which connect the *states* by determining the activity.

Fig. 7: Visualization of walking-falling followed by standing up from falling, sitting down, standing up and walking.

The individual vectorized training matrices $\text{vec}(Y_{\text{mD,train}})$, $\text{vec}(Y_{\text{RM,train}})$, and vectorized test matrices $\text{vec}(Y_{\text{mD,test}})$, $\text{vec}(Y_{\text{RM,test}})$ are used by the decision tree for μD and RM classification, respectively. Additionally, we apply the fusion classifier which uses the concatenated μD, $\text{vec}(Y_{\mu\text{D}})$, and RM, $\text{vec}(Y_{\text{RM}})$ vectors for the decision tree classifier, such as $Y_{\text{Fu}} = [\text{vec}(Y_{\mu\text{D}})^{\text{T}}, \text{vec}(Y_{\text{RM}})^{\text{T}}]^{\text{T}}$ [16], [21].

TABLE I: *Classifier 0 (away)*: First translation activity with (I) walking-stopping and (II) walking-falling away from the radar. Classifier: Decision tree; PC: $[d_{\mu\text{D}} = 3; d_{\text{RM}} = 3]$; $\sigma_{\text{mD,RM,Fu}} = [2.673\%, 3.624\%, 2.708\%]$; $\overline{P}_{\text{mD,RM,Fu}} = [\mathbf{92.24\%}, 84.47\%, 92.06\%]$, (Accuracy is expressed in %)

	Micro-Doppler predicted		Range-map predicted		Fusion predicted	
cl.	**(I)**	**(II)**	**(I)**	**(II)**	**(I)**	**(II)**
(I)	**92.1**	7.9	**85.6**	14.4	**92.1**	7.9
(II)	7.7	**92.3**	16.7	**83.3**	8.0	**92.0**

The highest average classification rate for μD ($P_{\mu\text{D}}$), RM (P_{RM}), or their fusion classification (P_{Fu}) is reported in each table. The standard deviation of 100 Monte Carlo simulation routines is expressed as $\sigma_{\text{mD,RM,Fu}}$ for the μD, RM, or fusion classification, respectively. The individual classification rates can be compared to Table V, which contains all ADL activities classified altogether at once. It is noted, a translation activity determined by the DTL resets the applied classifier, as shown in Fig. 6, such that the discrimination is executed only between walking-stopping or walking-falling in either direction.

For the first activity, the DTL has rendered the offset of the translating away activity, shown in Fig. 5a+5g for the μD and

TABLE II: *Classifier 0 (toward)*: Second translation activity with (I) walking-stopping and (II) walking-falling towards the radar. Classifier: Decision tree; PC: [$d_{\mu D} = 3$; $d_{RM} = 3$]; $\sigma_{mD,RM,Fu} = [1.918\%, 2.549\%, 1.969\%]$; $\overline{P}_{mD,RM,Fu} = [94.88\%, 89.78\%, \mathbf{95.03\%}]$, (Accuracy is expressed in $\%$)

	Micro-Doppler predicted		Range-map predicted		Fusion predicted	
cl.	**(I)**	**(II)**	**(I)**	**(II)**	**(I)**	**(II)**
(I)	**94.9**	5.1	**90.8**	9.2	**95.0**	5.0
(II)	5.1	**94.9**	11.2	**88.8**	5.0	**95.0**

the RM image. Here, a binary classifier 0 (away) is applied with the classes (I) walking-stopping and (II) walking-falling translating away from the radar. For translating away activities, the μD classification is used, since the average classification, $\overline{P}_{\mu D}$, rate has shown slightly higher performance than the fusion, $\overline{P}_{Fu}$ or even the RM, $\overline{P}_{RM}$, classifier, shown in Table I. Now, the ground truth activity of walking-stopping is correctly classified with 92.1% accuracy (compared to the all classes (aC) classifier in Table V: 89.6%).

Then the person turns around and translates towards the radar which is detected by the DTL. Thus a classifier reset is fulfilled. The previously classified activity of walking-stopping away from the radar does not affect any decision anymore, since the systems priority is the DTL. The rendered activity is shown in Fig. 5b+5h, which is classified with the binary *classifier 0 (toward)* (Table II) of (I) walking-stopping and (II) walking-falling towards the radar. For this classifier the dominant PC maintain with 3 and 3 for μD and RM, respectively. Differently from before, the fusion classification rate (μD+RM) is shown to outperform the μD and RM classifier. The ground truth motion of walking-falling is classified with 95.0% (aC: 92.5%) accuracy with 5.0% of false alarm probability and missing probability each. It is noted, the potentially life-threatening action of walking-falling can be overlooked by a probability of 5.0%. Therefore, the algorithm accounts for wrong decisions, as shown in Fig. 6 by the *state* blocks of standing and laying, which is then followed by the *Classifier 1*. This means the next activity can occur from a standing position, such as, (I) bending while standing, (II) sitting down facing the radar, (III) sitting down away from the radar with rotation, (IV) falling from standing. Or this can be from a laying position, such as, (V) standing up from falling, shown as *Classifier 1* in Table III. The first ground truth in-place activity of standing up from falling is rendered by the PBC, which is shown in Fig. 5c+5i. The PC changes to 4 and 2, whereas the fusion classifier keeps the highest average accuracy such that the ground truth activity is classified with 93.8% (aC: 82.4%). This activity then leads the person back to a standing position, where the same classifier is used again. The activity is discriminated by the PBC and is shown in Fig. 5d+5j. The ground truth action of (II) sitting down is classified with a certainty of 87.4% (aC: 74.7%). This activity leads the person to the sitting position, from where the *Classifier 2* is used with the classes (I) a standing up from sitting, (II) a standing up from sitting with rotation, and (III) a bending while sitting. The ground truth motion of standing up from sitting has 93.9% (aC: 72.9%) classification accuracy by using μD classification only (Table IV), which is superior over the fusion classification. The captured individual motion is shown in Fig. 5e and 5k. It is noted that we do not account for wrong decision at any given time, as performed in [18]; in fact, we rely on the proposed DTL approach, which resets the classifier after every translation activity. The follow-on actions are walking which is detected by the DTL where the detection routing is reset.

TABLE III: *Classifier 1*: The in-place activities of (I) bending while standing towards (T) the radar, (II) sitting down (T), (III) sitting down away (A) from the radar with rotation, (IV) falling from standing (T), (V) standing up from falling (T). Classifier: Decision tree; PC: [$d_{\mu D} = 4$; $d_{RM} = 2$]; $\sigma_{mD,RM,Fu} = [2.716\%, 2.806\%, 2.506\%]$; $\overline{P}_{mD,RM,Fu} = [86.38\%, 85.15\%, \mathbf{89.99\%}]$, (Accuracy is expressed in $\%$)

	Micro-Doppler predicted				
cl.	**(I)**	**(II)**	**(III)**	**(IV)**	**(V)**
(I)	**83.6**	10.0	2.7	2.9	0.8
(II)	11.7	**85.6**	1.8	0.7	0.1
(III)	3.5	2.3	**84.6**	5.0	4.6
(IV)	4.0	1.5	5.9	**87.4**	1.1
(V)	1.0	0.2	7.3	0.9	**90.6**
	Range-map predicted				
(I)	**78.3**	8.7	5.6	6.2	1.2
(II)	9.9	**86.2**	2.8	0.3	0.9
(III)	5.7	3.1	**83.3**	2.6	5.3
(IV)	8.0	0.3	2.9	**88.2**	0.6
(V)	2.5	1.6	5.1	1.1	**89.7**
	Fusion predicted				
(I)	**86.2**	8.2	2.6	2.4	0.6
(II)	10.7	**87.4**	1.5	0.3	0.1
(III)	3.7	2.3	**90.3**	1.4	2.3
(IV)	3.3	0.8	2.5	**92.3**	1.1
(V)	1.6	0.3	3.3	1.0	**93.8**

TABLE IV: *Classifier 2*: The in-place activities of (I) standing up from sitting (T), (II) standing up from sitting (T) with rotation, and (III) bending while sitting (T). Classifier: Decision tree; PC: [$d_{\mu D} = 3$; $d_{RM} = 2$]; $\sigma_{mD,RM,Fu} = [3.620\%, 4.740\%, 3.754\%]$; $\overline{P}_{mD,RM,Fu} = [\mathbf{88.80\%}, 77.28\%, 88.05\%]$, (Accuracy is expressed in $\%$)

	Micro-Doppler predicted			Range-map predicted			Fusion predicted		
cl.	**(I)**	**(II)**	**(III)**	**(I)**	**(II)**	**(III)**	**(I)**	**(II)**	**(III)**
(I)	**88.1**	0.5	11.5	**78.1**	4.1	17.8	**86.7**	0.5	12.8
(II)	1.7	**93.9**	4.4	4.5	**83.2**	12.3	1.4	**94.0**	4.6
(III)	11.7	3.9	**84.4**	17.6	11.9	**70.6**	12.5	4.0	**83.4**

IV. Conclusion

In this paper, we propose a simple yet effective approach based on the DTL to separate the human being's translational vs in-place activities. We found that a threshold of ± 0.15 for the DTL suits for bidirectionally translational and in-place activity separation. From a translational activity, we begin always with a binary classifier, which outperforms an ADL classifier with all 20 classes. The same applies for in-place activities, which enables us to drastically restrict the space to a small subset of possible activities at a given classification stage. For classification, the 2D-PCA is used to extract the features followed by a decision tree classifier. The method is

TABLE V: Fusion classifier for all ADL motion classes (all classes classifier – aC). Classifier: Decision tree; PC: [$d_{\mu D} = 4$; $d_{RM} = 3$]; $\sigma_{mD,RM,Fu} = [1.957\%, 2.053\%, 1.931\%]$; $\overline{P}_{mD,RM,Fu} = [72.80\%, 59.10\%, \mathbf{73.97\%}]$, (Accuracy is expressed in %)

Pred. Classes / True Classes	(I) Walking-Stopping-T	(II) Walking-Stopping-A	(III) Walking-Falling-T	(IV) Walking-Falling-A	(V) Bending w. Standing-T	(VI) Bending w. Standing-A	(VII) Sitting down-T	(VIII) Standing up f. Sitting-T	(IX) Sitting down-A	(X) Standing up f. Sitting-A	(XI) Sitting down w. Turning-T	(XII) Stand up f. Sitting w. turn-T	(XIII) Sitting down w. Turning-A	(XIV) Stand up f. Sitting w. turn-A	(XV) Bending w. Sitting-T	(XVI) Bending w. Sitting-A	(XVII) Falling. f. Standing-T	(XVIII) Standing f. Falling-T	(XIX) Falling. f. Standing-A	(XX) Standing f. Falling-A
I	**91.0**	0.4	8.1	0.6	0.0	0.0	0.0	0.0	0.0	0.0	0.0	0.0	0.0	0.0	0.0	0.0	0.0	0.0	0.0	0.0
II	0.7	**89.6**	0.3	9.5	0.0	0.0	0.0	0.0	0.0	0.0	0.0	0.0	0.0	0.0	0.0	0.0	0.0	0.0	0.0	0.0
III	6.9	0.3	**92.5**	0.3	0.0	0.0	0.0	0.0	0.0	0.0	0.0	0.0	0.0	0.0	0.0	0.0	0.0	0.0	0.0	0.0
IV	0.2	11.6	0.3	**87.9**	0.0	0.0	0.0	0.0	0.0	0.0	0.0	0.0	0.0	0.0	0.0	0.0	0.0	0.0	0.0	0.0
V	0.0	0.0	0.0	0.0	**62.4**	0.7	4.9	4.6	1.1	1.2	0.4	1.6	0.9	0.9	16.7	1.4	1.8	0.2	1.0	0.1
VI	0.0	0.0	0.0	0.0	1.1	**72.3**	1.0	0.9	7.1	4.8	0.2	0.5	2.5	1.7	0.6	6.5	0.3	0.1	0.2	0.2
VII	0.0	0.0	0.0	0.0	5.7	1.1	**74.7**	5.8	0.6	1.2	0.1	0.2	0.5	0.5	6.8	2.2	0.1	0.1	0.4	0.0
VIII	0.0	0.0	0.0	0.0	6.0	1.1	6.7	**72.9**	1.7	0.3	0.1	0.3	0.6	0.2	8.0	1.4	0.2	0.0	0.4	0.1
IX	0.0	0.0	0.0	0.0	1.7	8.8	1.1	1.9	**68.5**	2.3	0.5	0.5	5.1	1.1	1.4	5.1	1.1	0.1	0.2	0.7
X	0.0	0.0	0.0	0.0	1.7	5.7	1.6	0.6	1.9	**71.8**	0.1	0.4	2.0	6.3	0.9	5.0	0.3	0.4	1.2	0.1
XI	0.0	0.0	0.0	0.0	0.9	0.4	0.2	0.1	0.8	0.3	**70.9**	14.0	4.3	1.7	0.8	0.1	1.0	0.8	0.6	3.1
XII	0.0	0.0	0.0	0.0	1.7	0.6	0.2	0.5	0.9	0.5	13.6	**65.9**	4.0	2.4	1.3	0.2	0.6	2.8	1.8	2.9
XIII	0.0	0.0	0.0	0.0	1.7	3.4	0.8	1.0	6.0	2.8	4.1	4.0	**56.1**	8.9	0.7	2.0	1.3	1.2	1.5	4.4
XIV	0.0	0.0	0.0	0.0	1.5	2.3	0.7	0.5	1.6	7.1	2.2	3.2	9.4	**59.6**	0.3	1.7	1.0	5.5	0.9	2.6
XV	0.0	0.0	0.0	0.0	18.4	1.0	6.3	8.5	1.1	0.8	0.7	1.8	0.6	0.7	**57.1**	2.0	0.4	0.1	0.5	0.2
XVI	0.0	0.0	0.0	0.0	2.4	8.0	2.5	2.2	5.4	5.8	0.1	0.1	2.5	1.8	3.3	**64.1**	0.4	0.3	0.4	0.4
XVII	0.0	0.0	0.0	0.0	2.7	0.9	0.2	0.7	2.0	0.6	1.6	1.1	2.0	1.6	1.0	0.8	**81.7**	0.4	1.7	1.2
XVIII	0.0	0.0	0.0	0.0	0.2	0.4	0.1	0.1	0.1	0.4	0.7	3.4	1.7	5.8	0.1	0.5	0.2	**82.4**	0.6	3.2
XIX	0.0	0.0	0.0	0.0	2.0	0.8	0.9	0.2	0.5	2.6	0.7	2.0	1.1	2.3	0.6	1.1	1.5	0.7	**82.6**	0.4
XX	0.0	0.0	0.0	0.0	0.3	0.3	0.1	0.2	1.0	0.1	4.1	4.0	5.9	3.0	0.2	0.4	1.4	3.2	0.3	**75.6**

applied with different parameters (e.g. the number of principal components) or different data domains, e.g. micro-Doppler (μD) or the fusion classifier (μD and range classification at the same time). This provides initially promising results. Future work will extend this framework of hierarchical classification to more complex sequences of activities and more diverse positions of the available six radar sensors, as well as more subjects.

REFERENCES

[1] S. A. Shah and F. Fioranelli, "RF sensing technologies for assisted daily living in healthcare: A comprehensive review," *IEEE Aerospace and Electronic Systems Magazine*, vol. 34, no. 11, pp. 26–44, Nov 2019.

[2] F. Fioranelli, J. Le Kernec, and S. A. Shah, "Radar for health care: Recognizing human activities and monitoring vital signs," *IEEE Potentials*, vol. 38, no. 4, pp. 16–23, July 2019.

[3] F. Fioranelli, S. A. Shah, H. Li, A. Shrestha, S. Yang, and J. Le Kernec, "Radar sensing for healthcare," *Electronics Letters*, vol. 55, no. 19, pp. 1022–1024, 2019.

[4] B. Erol and M. G. Amin, "Radar data cube processing for human activity recognition using multi subspace learning," *IEEE Transactions on Aerospace and Electronic Systems*, pp. 1–1, 2019.

[5] J. Le Kernec, F. Fioranelli, C. Ding, H. Zhao, L. Sun, H. Hong, J. Lorandel, and O. Romain, "Radar signal processing for sensing in assisted living: The challenges associated with real-time implementation of emerging algorithms," *IEEE Signal Processing Magazine*, vol. 36, no. 4, pp. 29–41, July 2019.

[6] H. Li, X. Liang, A. Shrestha, Y. Liu, H. Heidari, J. Le Kernec, and F. Fioranelli, "Hierarchical sensor fusion for micro-gestures recognition with pressure sensor array and radar," *IEEE Journal of Electromagnetics, RF and Microwaves in Medicine and Biology*, pp. 1–1, 2019.

[7] A. Shrestha, H. Li, F. Fioranelli, and J. Le Kernec, "Activity recognition with cooperative radar systems at C and K band," *The Journal of Engineering*, vol. 2019, no. 20, pp. 7100–7104, 2019.

[8] Y. He, P. Aubry, F. Le Chevalier, and A. Yarovoy, "Decentralised tracking for human target in multistatic ultra-wideband radar," *IET Radar, Sonar Navigation*, vol. 8, no. 9, pp. 1215–1223, 2014.

[9] Y. He, P. Aubry, F. Le Chevalier, and A. Yarovoy, "Keystone transform based range-Doppler processing for human target in UWB radar," in *2014 IEEE Radar Conference*, 2014, pp. 1347–1352.

[10] M. G. Amin, A. Ravisankar, and R. G. Guendel, "RF sensing for continuous monitoring of human activities for home consumer applications," in *Big Data: Learning, Analytics, and Applications*, May 2019.

[11] S. A. Rane, A. Gaurav, S. Sarkar, J. C. Clement, and H. K. Sardana, "Clutter suppression techniques to detect behind the wall static human using UWB radar," in *2016 IEEE International Conference on Recent Trends in Electronics, Information Communication Technology (RTEICT)*, May 2016, pp. 1325–1329.

[12] A. Petroff, "A practical, high performance ultra-wideband radar platform," in *2012 IEEE Radar Conference*, 2012, pp. 0880–0884.

[13] B. Erol, M. Amin, F. Ahmad, and B. Boashash, "Radar fall detectors: a comparison," in *Radar Sensor Technology XX*, K. I. Ranney and A. Doerry, Eds., vol. 9829, International Society for Optics and Photonics. SPIE, 2016, pp. 349 – 357.

[14] S. Neemat, O. Krasnov, and A. Yarovoy, "An interference mitigation technique for FMCW radar using beat-frequencies interpolation in the STFT domain," *IEEE Transactions on Microwave Theory and Techniques*, vol. 67, no. 3, pp. 1207–1220, 2019.

[15] Y. He, P. Molchanov, T. Sakamoto, P. Aubry, F. Le Chevalier, and A. Yarovoy, "Range-Doppler surface: a tool to analyse human target in ultra-wideband radar," *IET Radar, Sonar Navigation*, vol. 9, no. 9, pp. 1240–1250, 2015.

[16] R. G. Guendel, "Radar classification of contiguous activities of daily living," Master Thesis, Villanova University, 2019, https://arxiv.org/abs/2001.01556.

[17] M. G. Amin and R. G. Guendel, "Radar classification of consecutive and contiguous human gross-motor activities," *IET Radar, Sonar & Navigation*, p. 12, 2020.

[18] M. G. Amin and R. G. Guendel, "Radar human motion recognition using motion states and two-way classifications," in *Proceedings of the 2020 IEEE Radar Conference (RadarConf)*, 2020.

[19] Jian Yang, D. Zhang, A. F. Frangi, and Jing-yu Yang, "Two-dimensional PCA: a new approach to appearance-based face representation and recognition," *IEEE Transactions on Pattern Analysis and Machine Intelligence*, vol. 26, no. 1, pp. 131–137, 2004.

[20] F. H. C. Tivive, S. L. Phung, and A. Bouzerdoum, "Classification of micro-Doppler signatures of human motions using log-Gabor filters," *IET Radar, Sonar Navigation*, vol. 9, no. 9, pp. 1188–1195, 2015.

[21] A. K. Seifert, L. Schäfer, M. G. Amin, and A. M. Zoubir, "Subspace classification of human gait using radar micro-Doppler signatures," in *2018 26th European Signal Processing Conference (EUSIPCO)*, 2018, pp. 311–315.